The ammonium transporter AmtB and the PII signal transduction protein GlnZ are required to inhibit DraG in *Azospirillum brasilense*

Vivian R. Moure[1], Catrine L. B. Siöberg[2], Glaucio Valdameri[1], Emmanuel Nji[2], Marco Aurelio S. Oliveira[1], Edileusa C. M. Gerdhardt[1], Fabio O. Pedrosa[1], David A. Mitchell[1] (iD), Lance C. Seefeldt[3], Luciano F. Huergo[1,4], Martin Högbom[2], Stefan Nordlund[2] and Emanuel M. Souza[1]

1 Instituto Nacional de Ciência e Tecnologia da Fixação Biológica de Nitrogênio, Departamento de Bioquímica e Biologia Molecular, Universidade Federal do Paraná, Curitiba, Brazil
2 Department of Biochemistry and Biophysics, Arrhenius Laboratories for Natural Sciences, Stockholm University, Sweden
3 Department of Chemistry and Biochemistry, Utah State University, Logan, UT, USA
4 Setor Litoral, Universidade Federal do Paraná, Matinhos, Brazil

The ammonium-dependent posttranslational regulation of nitrogenase activity in *Azospirillum brasilense* requires dinitrogenase reductase ADP-ribosyl transferase (DraT) and dinitrogenase reductase ADP-glycohydrolase (DraG). These enzymes are reciprocally regulated by interaction with the PII proteins, GlnB and GlnZ. In this study, purified ADP-ribosylated Fe-protein was used as substrate to study the mechanism involved in the regulation of *A. brasilense* DraG *in vitro*. The data show that DraG is partially inhibited by GlnZ and that DraG inhibition is further enhanced by the simultaneous presence of GlnZ and AmtB. These results are the first to demonstrate experimentally that DraG inactivation requires the formation of a ternary DraG-GlnZ-AmtB complex *in vitro*. Previous structural data have revealed that when the DraG-GlnZ complex associates with AmtB, the flexible T-loops of the trimeric GlnZ bind to AmtB and become rigid; these molecular events stabilize the DraG-GlnZ complex, resulting in DraG inactivation. To determine whether restraining the flexibility of the GlnZ T-loops is a limiting factor in DraG inhibition, we used a GlnZ variant that carries a partial deletion of the T-loop (GlnZΔ42-54). However, although the GlnZΔ42-54 variant was more effective in inhibiting DraG *in vitro*, it bound to DraG with a slightly lower affinity than does wild-type GlnZ and was not competent to completely inhibit DraG activity either *in vitro* or *in vivo*. We, therefore, conclude that the formation of a ternary complex between DraG-GlnZ-AmtB is necessary for the inactivation of DraG.

Introduction

Biological nitrogen fixation is the major route for conversion of dinitrogen gas (N_2) to ammonia in nature and it only occurs in some species of bacteria and archaea [1]. This process is catalyzed by the nitrogenase complex (hereafter referred as nitrogenase), which is composed of the metalloenzymes MoFe-protein (dinitrogenase) and Fe-protein (dinitrogenase reductase). Reduction of N_2 occurs in the active

Abbreviations
DraG, dinitrogenase reductase-activating glycohydrolase; DraT, dinitrogenase reductase ADP-ribosyl transferase; ITC, isothermal titration calorimetry; SPR, surface plasmon resonance.

site of the MoFe-protein, using electrons transferred from the Fe-protein [2]. In some diazotrophs, nitrogenase activity is regulated posttranslationally by ADP-ribosylation of one of the two subunits of the homodimeric Fe-protein. Such modification prevents the interaction between the Fe-protein and MoFe-protein, thereby inhibiting electron transfer and nitrogenase activity. This ADP-ribosylation is catalyzed by dinitrogenase reductase ADP-ribosyl transferase (DraT) upon a sudden increase in ammonium ions in the growth medium or following energy depletion (e.g., anaerobiosis). After ammonium exhaustion or energy level restoration, dinitrogenase reductase-activating glycohydrolase (DraG) catalyzes the removal of the ADP-ribosyl group, restoring nitrogenase activity. The signaling pathway leading to the regulation of nitrogenase by ammonium shock has been best described in the Alphaproteobacteria *Azospirillum brasilense* and *Rhodospirillum rubrum* and involves the signal transduction PII proteins, GlnB and GlnZ/GlnK [3–5].

The activities of DraT and DraG are regulated *in vivo* by interaction with PII signals [3]. These PII proteins are involved in the regulation of nitrogen metabolism, interacting with key protein targets in a conformation-dependent manner [6]. PII proteins share a homotrimeric structure of 12–13 kDa subunits, containing three flexible T-loops. The conformational states of PII proteins are governed by posttranslational modification and interaction with the effectors ADP, ATP, and 2-oxoglutarate (2-OG). In Proteobacteria, PII is posttranslationally modified by uridylylation at the Tyr-51 residue at low glutamine levels and deuridylylated at high levels of glutamine, with reactions being catalyzed by the bifunctional enzyme GlnD. ADP and ATP compete for binding sites located in the clefts between the subunits of the PII proteins [7,8]. Nucleotide binding is affected by the 2-OG levels: under nitrogen limitation, the levels of 2-OG increase, favoring the binding of ATP [8–11].

The current model for regulation of ADP-ribosylation in *A. brasilense* postulates an essential role for two PII proteins, GlnB and GlnZ. Thus, under nitrogen-fixing conditions, GlnB and GlnZ are uridylylated and are bound to ATP and 2-OG; in this state, GlnB does not interact with DraT, which is inactive in this state [12–14]. Under these conditions, the Fe-protein remains unmodified and, consequently, nitrogenase is active. In the presence of high ammonium, both GlnB and GlnZ are deuridylylated and are ADP-bound. In this conformational state, GlnB and GlnZ interact with DraT and DraG, respectively [12–15]. *In vitro* studies using purified proteins have shown that DraT is active when bound to GlnB, promoting ADP-

ribosylation of the Fe-protein and, thus, nitrogenase inactivation [16]. Under these conditions, the DraG-GlnZ complex moves toward the cytoplasmic membrane, forming a ternary complex with the membrane-bound AmtB, leading to DraG inhibition. However, the molecular mechanism leading to DraG inhibition remains elusive [12,14,15,17–19].

Structural modeling indicates that the interaction between GlnZ and DraG might inactivate DraG by preventing the binding of the ADP-ribosylated Fe-protein to the active site of DraG [18]. However, this simple model of DraG inactivation upon interaction with GlnZ is not supported by *in vivo* data; while the DraG-GlnZ complex is formed in an *amtB* knockout background, DraG is not inactivated in response to an ammonium shock in this background [12,17]. These results led to the hypothesis that AmtB stabilizes the DraG-GlnZ interaction and, thereby, it is required for effective DraG inactivation [18]. However, this hypothesis has not yet been experimentally confirmed.

Here, we used ADP-ribosylated Fe-protein as the substrate to study the regulation of *A. brasilense* DraG *in vitro*. The results show that GlnZ partially inhibits DraG and this inhibition is enhanced when GlnZ and AmtB are combined. This is the first experimental evidence that full DraG inactivation requires the formation of a DraG-GlnZ-AmtB ternary complex *in vitro*. We further analyzed the phenotype of a GlnZ variant carrying a deletion in the T-loop, GlnZΔ42-54. This variant binds to DraG with a slightly lower affinity than wild-type GlnZ and is not capable of fully inhibiting DraG activity either *in vitro* or *in vivo*. We conclude that the formation of a ternary DraG-GlnZ-AmtB complex is required for full inhibition of DraG in response to ammonium shock.

Results

DraG, GlnZ and AmtB expression predicted by mRNA expression

Reverse transcription quantitative PCR (RT-qPCR) was used to evaluate the mRNA levels of *nifH*, *glnB*, *draT*, *draG*, *amtB*, and *glnZ* in the wild-type strain under nitrogenase derepression conditions. We used the *draT*, *draG*, *glnZ* and *amtB* mRNA relative expression as a proxy for protein concentration ratios of DraT, DraG, GlnZ and AmtB (Table 1 and Fig. 1). The results indicate that the *glnZ* mRNA level is sevenfold higher than that of *draG*, suggesting a large excess of GlnZ and AmtB over DraG and DraT when *A. brasilense* FP2 cells were grown under nitrogen-fixing conditions. In addition to the mRNA expression,

Table 1. Sequence of gene-specific primers used in RT-qPCR analysis.

Azospirillum brasilense target genes

Gene	Gene product	ID (NCBI)	Sequence	Concentration[a]	Efficiency (threshold 0.4)
glnB	PII protein GlnB	GI:12698723	F 5′ TCACGAAGTCGGCATCAAGG 3′	200	1.91
			R 5′ TTCACCTTCGGCAGGAAGTC 3′		
amtB	Ammonium transporter AmtB	GI:3136067	F 5′ TGGTCAGCATCCTGTGGTTC 3′	800	1.93
			R 5′ TCAGGCTGTCCTTGGTGATG 3′		
glnZ	PII protein GlnZ	GI:3395451	F 5′ GTCGAGGCGATCCAGAAGG 3′	200	2.17
			R 5′ CAGAGAGCTTCGGTGTTGGT 3′		
draT	DraT	GI:142411	F 5′ TGCTGCCCACCTATCACAAG 3′	400	2.04
			R 5′ TCGAGCTGCAGGTTGATGTT 3′		
draG	Glicohydrolase (DraG)	GI:156465745	F 5′ CGACGAGTCGAACAAGCTCA 3′	400	2.08
			R 5′ TGACCGTCTGCATCGTATCG 3′		

Reference genes

| Reference	Abbreviation	Sequence	Concentration[a]	Efficiency (threshold 0.4)
[45]	*gyrA*	F 5′ TCACCGACGAAGAGTTGATG 3′	800	1.87
		R 5′ CTCTTCGATCTCGGTCTTGG 3′		
	glyA	F 5′ GGAGATCGCCAAGAAGATCA 3′	200	2.05
		R 5′ GCTCTTGGCGTAGGTCTTGA 3′		
	recA	F 5′ GTCGAACTGCCTGGTGATCT 3′	100	1.99
		R 5 GACGGAGGCGTAGAACTTCA ′3′		
[50]	*nifH*	F 5′ GCCCCGGAATTGAAGACA 3′	400	2.05
		R 5′ GCAATCTGGCGCAAAGACAT 3′		

[a](nM) of each primer in the PCR reaction.
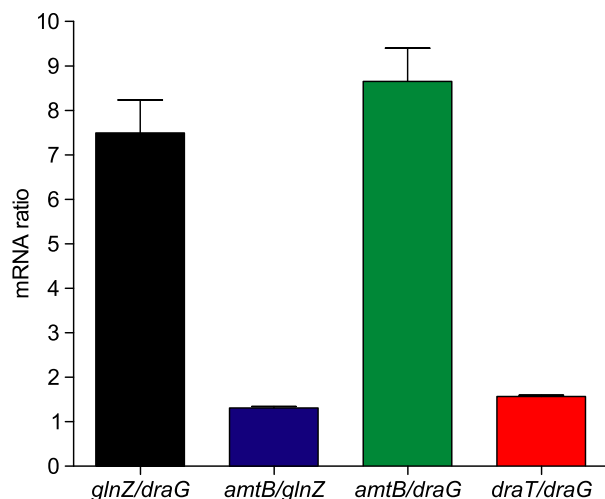
Fig. 1. mRNA ratio by RT q-PCR. Ratio values were determined using the calculated efficiency values and Ct value for each gene under nitrogen-fixing conditions, based on equation Ratio mRNA$_X$/mRNA$_Y$ = $Ef_X^{(Ct_X - Ct_X)}/Ef_Y^{(Ct_X - Ct_Y)}$, where X represents the numerator gene and Y the denominator gene. Data represent mean ± SD of three independent experiments performed in triplicates.

the *glnZ* gene ribosome binding site (RBS) sequence (AGGGGA) is more similar to the consensus sequence (AGGAGGA) than the *draG* RBS sequence (ACGGGA). Together, these results indicate that *in vivo* GlnZ levels are substantially higher than those of DraG.

Regulation of DraG activity

To assess whether the formation of the binary DraG-GlnZ or ternary DraG-GlnZ-AmtB complexes affects DraG activity, these complexes were reconstituted *in vitro* in the presence of ADP and the ADP-ribosyl hydrolase activity of DraG was determined by assessing the Fe-protein ADP-ribosylation pattern by western blot. The protein ratios used in these assays were based on the determined mRNA ratios (Fig. 1).

For these experiments, the substrate used was homodimeric ADP-ribosylated Fe-protein. Only one of the subunits is ADP-ribosylated, giving the double-band pattern observed in the control reaction without DraG (Fig. 2, lane NC). Addition of *A. brasilense* DraG resulted in the removal of the ADP-ribosyl moiety, as evidenced by the decrease in the intensity of the ADP-ribosylated band (Figs 2 and 3). The progressive

addition of GlnZ to the reaction to produce DraG to GlnZ ratios of 1 : 10 and 1 : 40 led to partial inhibition of DraG activity, by 18% and 40%, respectively (Fig. 2). The addition of AmtB further enhanced inhibition of DraG, resulting in up to ~ 70% DraG inhibition (Fig. 2). These data support the conclusion that the formation of a ternary complex involving DraG-GlnZ-AmtB is required to effectively inactivate DraG. The binding of AmtB to GlnZ was confirmed *in vitro* (Fig. 4).

Given the semiquantitative nature of the western blots used to probe DraG activity (Fig. 2), a more robust and quantitative assay was developed. In the next set of experiments, we probed DraG activity by analyzing its ability to reactivate purified ADP-ribosylated Fe-protein *in vitro*. For these assays, either GlnZ or a mixture of GlnZ and AmtB were incubated with DraG in the presence of ADP (to stimulate protein complex formation) and purified ADP-ribosylated Fe-protein (to act as substrate for DraG). After 20 min,

purified MoFe-protein was added to the reaction to assess nitrogenase activity by the H_2 evolution method [16]. Addition of GlnZ at a molar ratio of 1 : 40 (DraG : GlnZ) did not reduce DraG activity (Fig. 5). However, when AmtB was added to the reaction containing DraG and GlnZ, DraG activity was inhibited ~ 37%. This result clearly showed that nitrogenase reactivation (thus ADP-ribosyl removal) by DraG is inhibited in the presence of combined GlnZ and AmtB (Fig. 5).

It is worth noting that, in contrast to the results obtained by western blot (Fig. 2), the addition of GlnZ alone did not reduce DraG activity when the enzyme activity was probed by assaying nitrogenase activity directly (Fig. 5). Furthermore, the extent of DraG inhibition caused by GlnZ-AmtB was lower when DraG activity was probed in this assay in comparison to the western blot method (compare Figs 2 and 5). These differences may be explained by the fact that the DraG reaction was not stopped before
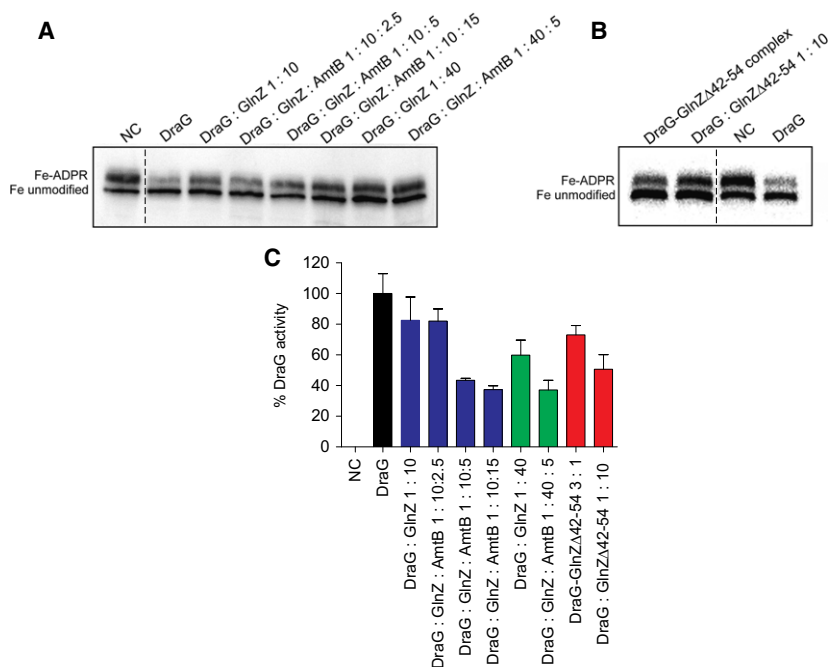

Fig. 2. Effect of GlnZ, AmtB (A), and GlnZΔ42-54 (B) on DraG activity. ADP-ribosylated Fe-protein was incubated with different purified proteins as indicated, or DraG-GlnZΔ42-54 complex obtained by co-purification. Reactions were carried out with 5 mM ADP and 3.5 µg of DraG. NC represents the reaction in the absence of DraG. The concentration ratios are indicated. (A) The molar ratios DraG : GlnZ : AmtB of lanes 3–8 correspond to ~ 1 : 10 : 2.5, 1 : 10 : 5, 1 : 10 : 15, 1 : 40, and 1 : 40 : 5, considering DraG as a monomer, and GlnZ and AmtB as trimers. (B) The molar ratios DraG : GlnZΔ42-54 of lane 1 correspond to 3 : 1, since the DraG-GlnZΔ42-54 was co-purified, lanes 2 and 3 correspond to 1 : 10 and 1 : 40 considering DraG as monomer and GlnZΔ42-54 as trimer. (C) Quantification of DraG activity in response to GlnZ, AmtB, and GlnZΔ42-54. The double band pattern of the NC in the absence of DraG is the fully ADP-ribosylated Fe-protein which contains both ADP-ribosylated Fe-protein (upper band) and unmodified Fe-protein band (lower band) at 1 : 1 ratio. In the reactions containing only DraG, we used an enzyme concentration that would allow ~ 50% reduction in the intensity of the ADP-ribosylated Fe-protein (upper band). Dotted lines on the blot images indicate the span positions of lanes removed from the same blot. Data represent mean ± SD of at least two independent experiments performed in triplicates.
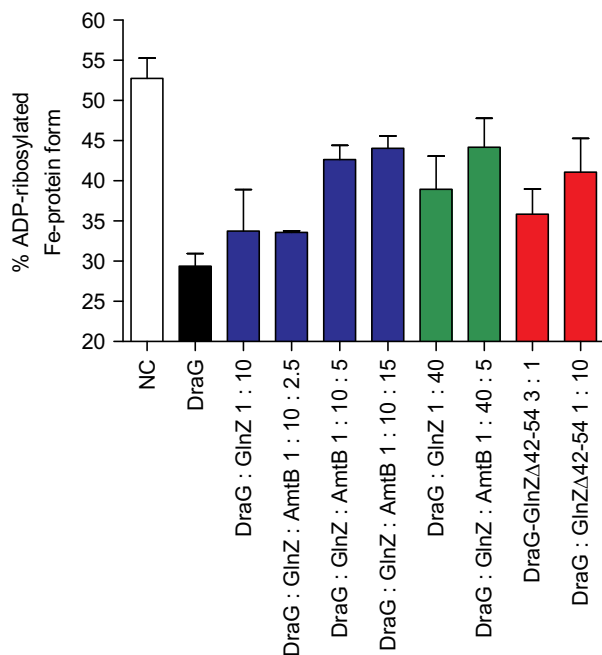
Fig. 3. Quantification of Fe-protein bands showing DraG activity in response to GlnZ, AmtB, and GlnZΔ42-54. The bands observed in the western blot for Fe-protein, corresponding to unmodified and ADP-ribosylated forms of Fe-protein, were quantified using the IMAGEJ program. NC corresponds to the reaction in the absence of DraG. Data represent mean ± SD of at least two independent experiments.

coupling to the nitrogenase activity. Consequently, when ATP was added to allow nitrogenase activity, the DraG-GlnZ or DraG-GlnZ-AmtB would partially disrupt [15], allowing free DraG to reactivate the ADP-ribosylated Fe-protein.

In contrast to all known structures of PII proteins complexed to their targets, the interaction of DraG

with GlnZ does not require the GlnZ T-loop. Although the GlnZ T-loop is highly flexible and could not be modeled in the previously determined DraG-GlnZ crystal structure [18], the interaction with DraG is expected to restrict the mobility of the T-loop, as more conformations will be forbidden within the DraG-GlnZ [20]. This mode of interaction allows DraG and GlnZ to form a complex with AmtB, in which the GlnZ T-loops participate and become ordered, by analogy with the AmtB-GlnK complex [18,21]. A restriction of the mobility of the T-loops during the AmtB-GlnZ interaction may thus enhance the stability of DraG-GlnZ within the DraG-GlnZ-AmtB ternary complex.

If these assumptions are correct, GlnZΔ42-54, which is a GlnZ variant carrying a partial deletion of the T-loop, should form a more stable complex with DraG, even in the absence of AmtB. We hypothesized that GlnZΔ42-54 could potentially bypass the requirements of forming a ternary complex with AmtB to effectively inactivate DraG. Indeed, *in vitro* assays indicated that GlnZΔ42-54 was more effective than native GlnZ to inactivate DraG in the absence of AmtB (at a 1 : 10 DraG : GlnZ ratio, GlnZΔ42-54 inhibited DraG activity up to 50% while only 18% of DraG inhibition was observed when native GlnZ was used, Fig. 2A,B).

The structure of the DraG-GlnZΔ42-54 complex

To gain insight into the structural basis for the inhibition of DraG by GlnZΔ42-54, we solved the crystal structure of this complex. The DraG-GlnZΔ42-54 complex was crystallized and the X-ray structure was determined at 1.55 Å resolution ($R_{work} = 14.4\%$, $R_{free} = 16.5\%$) by molecular replacement using the DraG-GlnZ complex as search model. The structure
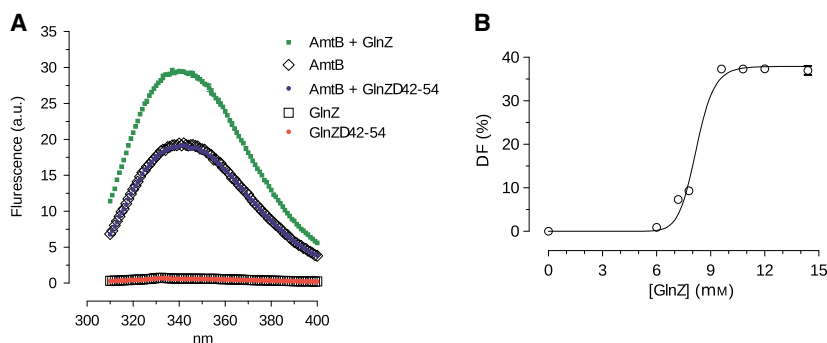

Fig. 4. Binding of GlnZ to AmtB. (A) Emission spectra for *Escherichia coli* AmtB at a concentration of 1.5 μM (considering the molecular weight of the AmtB trimer as 134 kDa), in the presence of GlnZΔ42-54 (7.8 μM) or GlnZ (7.2 μM), 0.03% DDM, 5 mM ADP, and 10 mM MgCl₂. As control, GlnZΔ42-54 and GlnZ alone were used. (B) Saturation curve of GlnZ binding with AmtB, yielding a K_D of 8.2 ± 0.1 μM using the GRAPH PAD PRISM program. All emissions were measured at 300 nm.
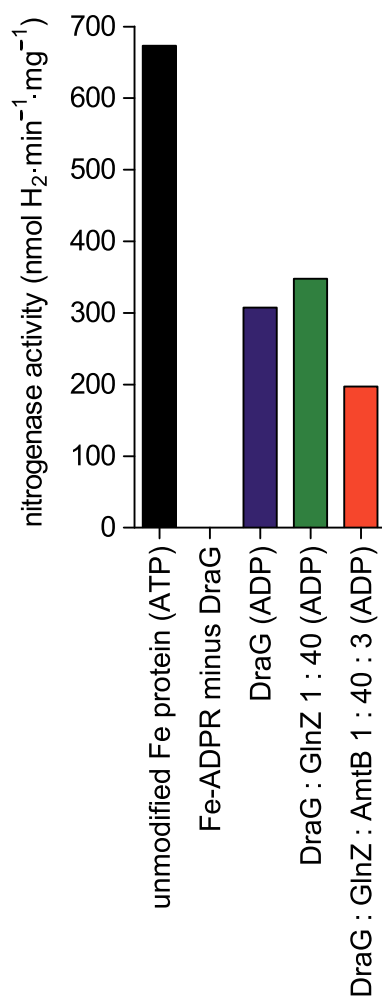
Fig. 5. Effect of GlnZ and AmtB on DraG activity through *Azotobacter vinelandii* Fe-protein reactivation. DraG activity was assessed indirectly from Fe-protein activity by measuring hydrogen evolution. Reaction mixtures for the DraG assay contained 50 mM MOPS pH 7.5, 10 mM $MgCl_2$, 1 mM $MnCl_2$, 5 mM ADP or ATP, 0.03% TX, 150 µg of *in vitro* ADP-ribosylated Fe-protein, and 10 µg of DraG, either alone or in the presence of GlnZ (trimer) and AmtB (trimer) from *Azospirillum brasilense* at the indicated molar ratio. For the nitrogenase activity control, unmodified Fe-protein activity was measured in the presence of 0.03% TX. The Fe-protein activity was determined by adding 500 µg of MoFe-protein and measuring H_2 evolution.

Table 2. Data collection and refinement statistics. Values in parentheses are for highest resolution shell.

Data collection statistics	
Space group	H3
Cell dimensions (Å)	$a = b = 116.7$,
	$c = 105.6$
Resolution (Å)	1.55 (1.63–1.55)
R_{merge}	0.103 (0.727)
Mean $(I)/\sigma(I)$	10.9 (2.1)
Completeness (%)	100 (100)
Wilson B-factor (Å^2)	11.5
Refinement statistics	
Resolution (Å)	45.6–1.55
No. reflections work/test set	70 135/3881
R_{work}/R_{free} (%)	14.4/16.5
Rmsd from ideal bonds (Å)/angles (°)	0.025/2.44
Ramachandran zone distribution (%) favored/allowed/outliers	98/2/0

from Gln42 to Ser54 of the T-loop were confirmed to be absent. The structure in this region of GlnZ is now well ordered with clear density for all residues, including the peptide bond between Gly41 and Phe55.

The structure of the DraG-GlnZΔ42-54 complex confirmed the previous suggestion that the ADP-ribosylated Fe-protein cannot access the DraG active site due to steric hindrance. Interestingly, an ADP molecule was bound in the ADP-ribose binding site of DraG, interacting with conserved residues involved in both catalysis (Asp60) and binding of ADP-ribose (Thr101, His158, and Tyr212) [23] (Fig. 7), which was not observed in previous DraG structures. The mode of ADP binding described here resembles the ADP binding molecular model in previous DraG structures [22] and the binding of ADP-ribose crystalized with DraG [23].

Thermodynamic and kinetic analysis of the DraG-GlnZ and DraG-GlnZΔ42-54 complexes

We used isothermal calorimetry (ITC) to determine if GlnZΔ42-54b could form a more stable complex with DraG than with the native GlnZ-DraG complex. These experiments were performed in the presence of saturating ADP (3 mM) since both DraG and GlnZ bind this nucleotide, which is also required for protein complex formation. In both the GlnZ-DraG and the GlnZΔ42-54-DraG complexes, the binding was exothermic and the titration curves were fitted using a one-to-one binding model without cooperativity, giving K_D values of 3.4 and 8.1 µM for GlnZ and GlnZΔ42-54, respectively (Table 3 and Fig. 8). The K_D of the DraG-GlnZ complex described here is in good agreement with previous data (3.4 vs 1.5 µM) [18]. The

shows no significant changes in the DraG structure or the DraG-GlnZ interaction interface compared to the previously published structures [18,22] (Table 2 and Fig. 6). In the previous DraG-GlnZ structure, only the N-terminal region of the T-loop from Gly37 to Lys40 is modeled; the residues from Gly41 to Ser52 are not visible in the electron density, presumably due to disorder [18]. The crystal structure of DraG-GlnZΔ42-54 showed residue Gly41 and, as expected, the residues
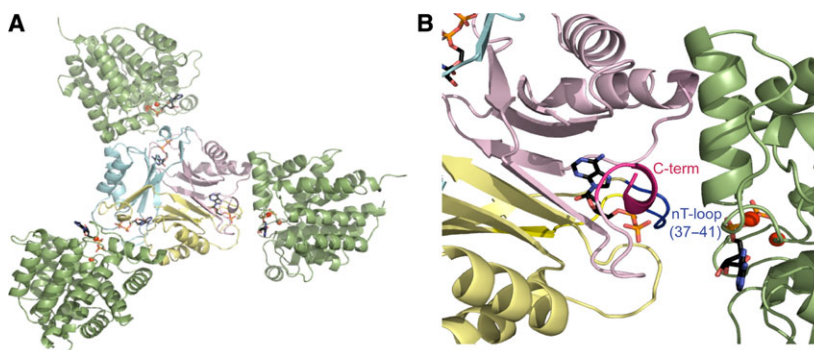
Fig. 6. DraG-GlnZΔ42-54 complex structure. The partial deletion of the T-loop of GlnZ (Q42-S54) does not affect its interaction with DraG. (A) Cartoon representation of DraG monomers (green) interacting with each monomer of GlnZΔ42-54 (light pink, yellow, and cyan). Mg^{2+} ions are shown as red spheres. ADP is shown in black sticks. The ADP is bound in the lateral clefts between the GnZΔ42-54 subunits and in the DraG ADP-ribose site. The crystal structure was obtained in the presence of 1 mM ADP. (B) DraG-GlnZΔ42-54 interface. Specific regions of the GlnZΔ42-54 monomer that interact with DraG are shown in dark pink, corresponding to residues 22–25 and the C-terminal region. The N-terminal region of the T-loop is shown in dark blue to emphasize its participation in the interaction with DraG.
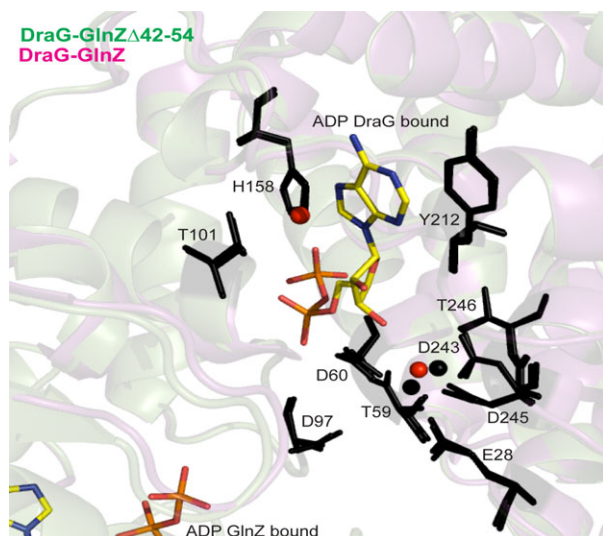

Fig. 7. ADP binding to DraG. Structural alignment of DraG-GlnZΔ42-54 (green) and DraG-GlnZ (pdb 3O5T in magenta). Mg^{2+} ions are shown as red and black spheres in DraG-GlnZΔ42-54 and DraG-GlnZ, respectively. ADP is shown in yellow sticks. Amino acids involved in the binding site of the ADP-ribosyl moiety, metal binding and catalysis are shown as black sticks.

results indicate that GlnZΔ42-54 forms a less stable complex with DraG than does the native protein.

In both DraG-GlnZ and DraG-GlnZΔ42-54, complex formation was favored by both enthalpy and entropy changes (Table 3). However, the formation of the GlnZ-DraG complex was mostly driven by enthalpy (Table 3) while the formation of the DraG-GlnZΔ42-54 complex had similar contributions from enthalpy and entropy (Table 3). These differences are

consistent with the hypothesis that the disordered T-loop of GlnZ imposes a greater entropic penalty upon interaction with DraG than occurs with GlnZΔ42-54 [24–26].

In order to determine the kinetic properties of these protein complexes, surface plasmon resonance spectroscopy (SPR) was performed. DraG was immobilized and titrated with either GlnZ or GlnZΔ42-54 in the presence of ADP. The results are shown in Fig. 9 and summarized in Table 4. The SPR data corroborate the ITC analysis and indicate only minor differences in the affinity of DraG for GlnZΔ42-54 compared with GlnZ.

In vivo effects of GlnZΔ42-54 on DraG regulation

The effect of GlnZ and AmtB on DraG activity has been studied in *A. brasilense* [13,17,27], *Rhodobacter capsulatus* [28], *Azoarcus* sp. [29], and *R. rubrum* [4,30]. As previously reported [17], and confirmed here, the Fe-protein modification in response to the addition of ammonium was slightly faster in the *A. brasilense glnZ* mutant than in the wild-type FP2 and it was defective in the *amtB* mutant (Fig. 10). The reason for the slightly faster response in the *glnZ* strain is unknown; in *A. brasilense*, the absence of GlnZ does not affect glutamine synthetase activity or GlnB expression [3,6].

The *A. brasilense* 7611 (*glnZ* mutant) and FAJ310 (*amtB* mutant) strains carrying the plasmids pLAFRglnZ or pLAFRglnZΔT, expressing GlnZ or GlnZΔ42-54 (from the constitutive *lac* promoter and containing a strong RBS site derived from the pET28a vector), were subjected to an ammonium shock and

Table 3. Thermodynamic parameters for the binding of DraG to GlnZ or GlnZΔ42-54 at 298 K.

Analyte	N	K_D (µM)	ΔH (kcal·mol^{-1})	$T\Delta S$ (cal·mol^{-1}·K^{-1})	ΔG (kcal·mol^{-1})
GlnZ	1.35	3.4	−5372	−2085	−7457
GlnZΔ42-54	0.99	8.1	−3127	−3814	−6941
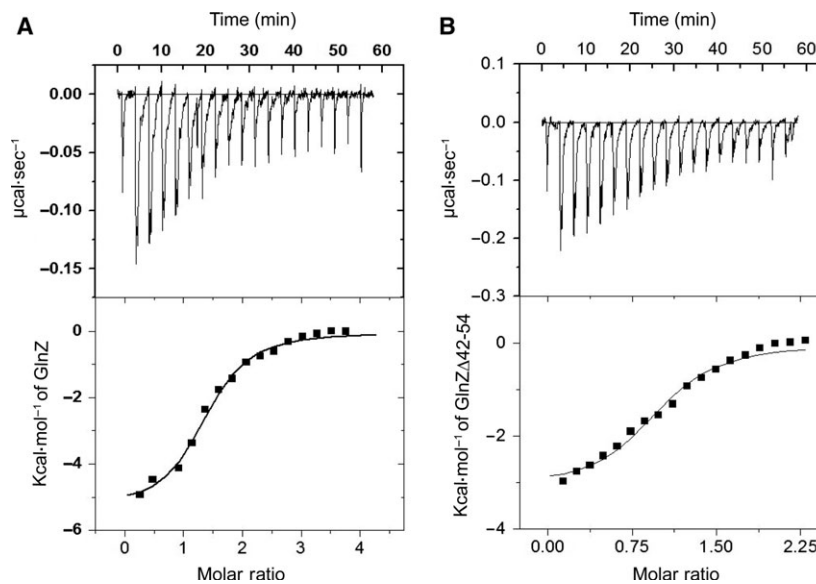
Fig. 8. Isothermographs of DraG interaction with GlnZ (A) and GlnZΔ42-54 (B). All proteins were saturated with ADP. All experiments were performed at 25 °C in the presence of 10 mM Mg^{2+} and 3 mM ADP and could be described with a one-set-of-sites model.
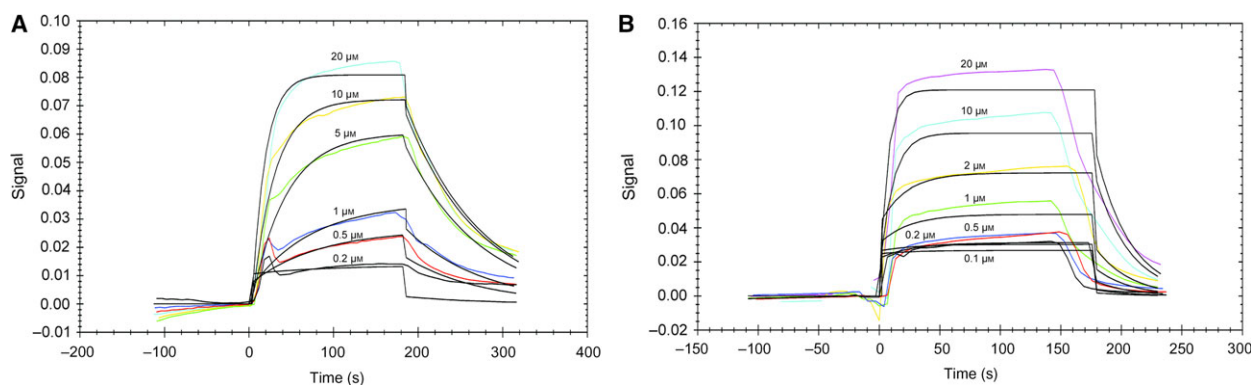
Fig. 9. Analysis of DraG binding to GlnZ (A) and GlnZΔ42-54 (B) by SPR. The sensorgrams show the relative response for interactions between immobilized DraG when protein partners were injected at varied concentrations (0.1–20 µM). In the sensorgrams, experimental curves are shown in colors and the fitting curves are shown in black. The best fitting model adopted by the TRACE DRAWER™ software (Ridgeview Instruments AB, Uppsala, Sweden) was used to determine the affinity constants and binding kinetics.

the dynamics of Fe-protein ADP-ribosylation were assessed by western blot using anti-NifH antibody. Comparison of the Fe-protein ADP-ribosylation profiles showed that the Fe-protein was kept longer in the modified form in 7611 cells carrying either pLAFRglnZ or pLAFRglnZΔT (Fig 10, compare 7611 with or without plasmids at 14 and 16 min), suggesting that DraG inhibition after the addition of ammonium is more effective when GlnZ or GlnZΔ42-54 is overexpressed from a plasmid.

A faint signal of ADP-ribosylated Fe-protein is always observed at time zero in the *draG* null background [31]. Given that no signal of ADP-ribosylated Fe-protein was detected at time zero before the addition of ammonium (Fig. 10), we conclude that DraG is still subject to regulation when GlnZ is overexpressed, that is, DraG is not locked in an off state upon GlnZ overexpression.

Interestingly, although weak and delayed, it was possible to detect a faint band of ADP-ribosylated Fe-

Table 4. Association and dissociation rate constants and binding affinities of GlnZ and GlnZΔ42-54 to DraG.

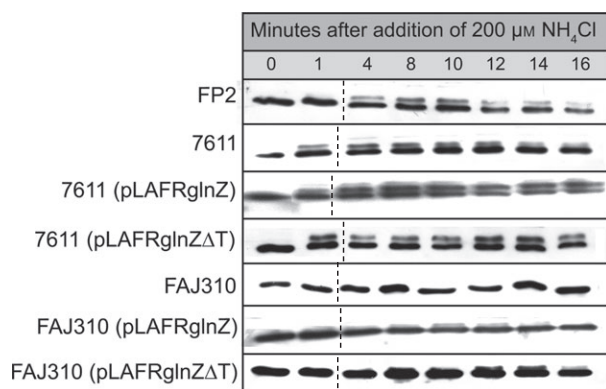| Protein	k_{on} (M^{-1}·s^{-1})	k_{off} (s^{-1})	K_D (μM)
GlnZ	$2.65 \times 10^3 \pm 6.41 \times 10^1$	$1.13 \times 10^{-2} \pm 6.69 \times 10^{-7}$	4.26 ± 0.10
GlnZΔ42-54	$5.98 \times 10^3 \pm 4.73 \times 10^2$	$3.52 \times 10^{-2} \pm 4.58 \times 10^{-6}$	5.88 ± 0.47

Fig. 10. *In vivo* effect of GlnZ and GlnZΔ42-54 on Fe-protein modification. Modification of Fe-protein in *Azospirillum brasilense* FP2, 7611 (*glnZ* mutant), and FAJ310 (*amtB* mutant) was used as control, 7611 (pLAFRglnZ) and FAJ310 (pLAFRglnZ) express GlnZ, and 7611 (pLAFRglnZΔT) and FAJ310 (pLAFRglnZΔT) express GlnZΔ42-54. To the cells derepressed for nitrogenase, 200 μM NH₄Cl was added at zero time. Cell extracts were removed at specific times and analyzed using SDS/PAGE followed by western blot using anti-NifH antibody. Dotted lines on the blot images indicate the span positions of lanes removed from the same blot.

protein in the FAJ310 *amtB* strain overexpressing either GlnZ or GlnZΔ42-54 (Fig 10, compare FAJ310 with or without plasmids at 10 and 14 min). These data suggest that DraG can be partially inhibited by GlnZ or GlnZΔ42-54 in the absence of AmtB when GlnZ is overexpressed, in good agreement with our *in vitro* findings (Fig. 2).

Discussion

In this work, we determined the functional significance of the formation of the DraG-GlnZ and DraG-GlnZ-AmtB complexes in the regulation of DraG activity by assessing its activity *in vitro* using its natural substrate, the ADP-ribosylated Fe-protein. We showed that GlnZ is able to partially inhibit DraG activity *in vitro* in a dose-dependent manner (Fig. 2). However, the inhibition of DraG by GlnZ is modest and could not explain the tight regulation of the Fe-protein ADP-ribosylation cycle observed *in vivo* (Fig. 10). Our data

clearly show that only the combined presence of GlnZ and AmtB results in a degree of inhibition (~ 70%) of DraG *in vitro* that could account for the observed response *in vivo* (Figs 2, 5 and 10). Hence, our data provide the first *in vitro* experimental support for the hypothesis that the formation of a DraG-GlnZ-AmtB complex is required for effective DraG inactivation in response to ammonium.

In living cells, the formation of the DraG-GlnZ-AmtB ternary complex on the membrane would lead to the physical separation of DraG from its cytoplasmic substrate; this separation was presumed to be an indispensable feature of the mechanism for DraG inhibition upon ammonium shock [17]. Given that we detected effective DraG inhibition in the presence of AmtB and GlnZ *in vitro* (Figs 2 and 3), it is more likely that DraG inhibition does not require the physical separation of the enzyme from its substrate.

The structure of the DraG-GlnZ complex led previously to the hypothesis that DraG inhibition results from steric hindrance of its active site by GlnZ [18]. However, GlnZ was not capable of inhibiting DraG activity toward dansyl-arginine-ADP-ribose, an artificial low-molecular-weight substrate of DraG [18]. Our current hypothesis is that the DraG-GlnZ complex is not stable enough *in vivo* to effectively inhibit DraG. The further engagement of AmtB to form a ternary DraG-GlnZ-AmtB complex would be required to enhance the apparent affinity of the DraG-GlnZ interaction thereby allowing effective inhibition of DraG [17,18,20].

The presumed instability of the binary DraG-GlnZ complex could be due to the conformational restriction of the highly flexible GlnZ T-loops upon DraG binding causing an entropic penalty during the formation of the DraG-GlnZ complex [18]. In an attempt to address this question, we used a GlnZ variant carrying a partial deletion of the T-loop (GlnZΔ42-54). Although the GlnZΔ42-54 variant inhibited DraG slightly more effectively than did native GlnZ (Fig. 2), it was not able to compensate for the absence of AmtB either *in vitro* or *in vivo* (Figs 2 and 10). Indeed, the binding affinity of GlnZΔ42-54 to DraG was very similar to that of wild-type GlnZ to DraG (Tables 3 and 4). Furthermore, no significant differences in the protein interaction interface

were observed in the structure of the GlnZΔ42-54-DraG complex (Fig. 6). These data support the conclusion that the GlnZ T-loop is not a major determinant of the binding affinity and refute our original hypothesis that the deletion of the T-loop would lead to stabilization of the DraG-GlnZ complex.

In summary, we conclude that the formation of the ternary DraG-GlnZ-AmtB complex is required for the full inhibition of DraG toward its natural substrate, ADP-ribosylated Fe-protein. Therefore, in the ternary complex, DraG is hindered from accessing its natural substrate.

Materials and methods

Preparation of *Rhodospirillum rubrum* ADP-ribosylated Fe-protein

Rhodospirillum rubrum S1 was grown photoheterotrophically at 30 °C in minimal media as previously described [32] using 28 mM ammonium chloride (i.e., in nitrogen-rich conditions). Nitrogen-fixing conditions were established by sparging with 5% CO_2 in 95% N_2 as nitrogen source. Nitrogenase activity was measured by acetylene reduction. The culture was subjected to ammonium shock by addition of 20 mM ammonium chloride for 20 min in order to promote ADP-ribosylation of the Fe-protein. Cells were anaerobically harvested by centrifugation at 3000 *g* for 15 min and frozen in liquid nitrogen until further use. Cell pellets (about 4 g wet weight·L^{-1} culture) were resuspended in degassed buffer 100 mM Tris pH 7.5 and 1 mM dithionite supplemented with DNAse (final concentration of 20 U·mL^{-1}) and one tablet of complete EDTA-free protease inhibitor (Roche, Indianapolis, IN, USA) for each 50 mL of extract (3 mL buffer·g^{-1} wet weight of cell pellet). Lysis was performed by passing the cell suspension twice through a French Pressure Cell, at 18000 psi. The cell lysate was centrifuged at 200 000 *g* for 90 min, to separate the membrane fraction from the *R. rubrum* extracts containing ADP-ribosylated Fe-protein. The extracts were frozen in liquid nitrogen and stored at −80 °C until use.

Protein expression and purification

Azospirillum brasilense GlnZ, GlnZΔ42-54, DraG, and His-tagged DraG were produced in *Escherichia coli* strain BL21 (DE3) harboring the plasmids pMSA4 [33], pMSA4Δ42-54 [18], pLHPETdraG [31], and pLHPETdraGwt [13], respectively. For expression, freshly transformed *E. coli* was used to inoculate overnight cultures of Luria Bertani (LB) medium supplemented with 50 μg·mL^{-1} kanamycin. Aliquots of 10 mL of each overnight culture were used to start the 1-L expression cultures that were grown to an OD_{600} of 0.6. Cells were induced with 0.4 mM IPTG (Sigma, St. Louis, MO, USA) for 4 h at 37 °C for production of PII proteins (GlnZ and GlnZΔ42-54) and overnight at 20 °C for DraG and His-tagged DraG. Cells were harvested by centrifuging at 4000 *g* for 10 min at 4 °C and stored at −80 °C until use.

PII proteins were purified using a thermal treatment at 70 °C for 15 min prior to loading on a 5-mL HiTrap heparin column (GE HealthCare, Little Chalfont, Buckinghamshire, UK) and eluted with a nonlinear KCl gradient as previously described [33]. DraG was also purified using 5-mL HiTrap heparin columns and eluted with a nonlinear gradient of NaCl [13]. The proteins were dialyzed in buffer containing 20 mM Hepes pH 7.5, 100 mM KCl (for PII proteins), or 100 mM NaCl (for DraG) and 10% glycerol and then concentrated by centrifuge ultrafiltration (10 kDa MWCO; Sartorius Stedim Biotech, Goettingen, Germany) to ∼ 15 mg·mL^{-1}, determined by the Bradford method. His-tagged DraG was purified using a 1-mL His-Trap column (GE HealthCare) and eluted with a nonlinear gradient of imidazole, as described previously [31], and then dialyzed in buffer with 50 mM Tris pH 7.5, 100 mM NaCl, and 30% glycerol. *Azospirillum brasilense* AmtB was purified as previously described [19], using *E. coli* GT1000 cells harboring pLHDK7HisAmtB plasmid.

Escherichia coli AmtB was produced in *E. coli* Lemo21 (DE3) harboring an AmtB-GFP$_{8His}$ fusion construct. This fusion construct was obtained from a GFP fusion library [34]. The fusion protein was cloned into the expression vector, pWaldo GFPd [35]. For expression, freshly transformed *E. coli* was used to inoculate 60 mL of LB medium supplemented with 50 μg·mL^{-1} kanamycin and was grown at 37 °C for 16 h. The culture was then used to inoculate six flasks of 1 L of MemStar medium [36] and grown to an OD_{600} of 0.6, and AmtB-GFP$_{8His}$ superexpression was induced with 0.4 mM IPTG overnight at 25 °C. Cells were harvested by centrifuging at 4000 *g* for 10 min at 4 °C and resuspended in 200 mL of ice-cold 1× PBS buffer, flash frozen in liquid nitrogen and stored at −80 °C until use.

Membranes containing AmtB-GFP$_{8His}$ from 6 L of culture were isolated after breaking the cells using a Constant Cell Disruption system (2 × 25 000 psi passes at 4 °C). The unbroken cells and debris were removed by centrifuging at 10 000 *g* for 10 min at 4 °C. The supernatant containing the AmtB-GFP$_{8His}$ was centrifuged at 150 000 *g* for 1 h at 4 °C and the green pellets were resuspended in 60 mL of ice-cold 1× PBS buffer. The resuspended membranes (30 mL in 2 × 50 mL tube each) were flash frozen in liquid nitrogen and stored at −80 °C until use. AmtB-GFP$_{8His}$ was purified using the published protocol [35]. Briefly, the membrane fraction was added to 300 mL of solubilization buffer (SB) containing 150 mM NaCl, 1× PBS pH 7.5, 10% (v/v) glycerol, and 1% (w/v) *n*-dodecyl-β-D-maltoside (DDM) and was incubated for 1 h at 4 °C with gentle stirring. The non-solubilized membranes were removed by ultracentrifugation at 120 000 *g* for 1 h at 4 °C. The supernatant containing the solubilized proteins

was incubated at 4 °C with Ni^{2+}-NTA resin (Qiagen, Hilden, Germany) for 2 h with gentle stirring. To exclude unspecific binding, 10 mM imidazole was added. After batch binding for 2 h, the slurry was poured onto a 300 mL gravity Econo column (BioRad, Hercules, CA, USA) and step washed with 20 column volumes of SB containing 10, 20, and 30 mM imidazole. The AmtB-GHP$_{8His}$ was eluted using SB containing 250 mM imidazole. The eluted sample was dialyzed with His-tag TEV protease [37] at 4 °C in buffer containing 20 mM Tris pH 7.5, 150 mM NaCl, and 0.03% (w/v) DDM (1 mg of AmtB-GFP$_{8His}$ with 1 mg of TEV). After the TEV cleavage, the His-tag TEV protease, free GFP$_{8His}$, and uncleaved AmtB-GFP$_{8His}$ were removed by passing the samples through a 5-mL His-Trap column (GE Healthcare). The flow-through (40 mL) containing AmtB was concentrated to 500 µL using centrifuge filtration units of 100 kDa MWCO (Sartorius Stedim Biotech) and was then injected onto a Superose 200 10/300 column (GE Healthcare) at a flow rate of 0.4 mL·min^{-1} using buffer containing 20 mM Tris pH 7.5, 150 mM NaCl, and 0.03% (w/v) DDM at 4 °C. The AmtB sample after gel filtration was concentrated to 4 mg·mL^{-1}.

Formation of the binary DraG-PII and ternary DraG-PII-AmtB-reconstituted complexes *in vitro*

Purified proteins (DraG and GlnZ or GlnZΔ42-54 and *E. coli* AmtB) were incubated with 50 mM Hepes pH 7.5, 10 mM MgCl$_2$, 2 mM MnCl$_2$, 1 or 5 mM ADP, and 0.03% (w/v) DDM at 4 °C overnight, using the indicated molar ratios, considering DraG as a monomer, and GlnZ and AmtB as trimers.

DraG-GlnZΔ42-54 complex formation for crystallization assays

GlnZΔ42-54 and DraG were purified separately. They (0.8 µmol of each) were incubated with 20 mM Hepes pH 7.5, 100 mM NaCl, 10 mM MgCl$_2$, and 5 mM ADP at 4 °C overnight. The mixture was loaded on a Superdex 200 16/60 column and the complex was eluted as a single symmetrical peak corresponding to ~ 100 kDa, using 20 mM Hepes pH 7.5, 100 mM NaCl, 5 mM MgCl$_2$, 1 mM ADP, and 5% glycerol. The DraG-GlnZΔ42-54 complex was concentrated in a 30 kDa MWCO centrifuge filtration unit (Sartorius Stedim Biotech) to ~ 7.8 mg·mL^{-1}, determined by the Bradford method, and was then flash frozen in liquid nitrogen and stored at −80 °C until use.

Determination of DraG activity *in vitro*

The reaction mixture contained 50 mM Hepes pH 7.5, 2 mM MnCl$_2$, 10 mM MgCl$_2$, 1 or 5 mM ADP, 0.03% (w/v) DDM, and the indicated amounts of DraG, the DraG-GlnZ binary or the DraG-GlnZ-AmtB ternary complexes. The reaction

was initiated by the addition of *R. rubrum* ADP-ribosylated Fe-protein under anaerobic conditions, followed by incubation at 30 °C, 130 r.p.m. for 20 min. The reaction was terminated by the addition of SDS/PAGE loading buffer followed by immediate boiling. The level of ADP-ribosylation of the Fe-protein was determined by SDS/PAGE, as described previously [38], followed by western blotting and revelation with antibody against the *R. rubrum* Fe-protein. To determine the effects of GlnZ, AmtB, and GlnZΔ42-54 on DraG activity, fully ADP-ribosylated Fe-protein, which produces a double-band pattern on SDS/PAGE, was used as substrate. The upper band corresponds to ADP-ribosylated Fe-protein. The fully ADP-ribosylated Fe-protein was taken as a negative control (NC) in the absence of DraG and corresponds to 0% of DraG activity. The amount of DraG (0.012 mg·mL^{-1} or 0.38 µM) promoting a 50% decrease in the intensity of the ADP-ribosylated Fe-protein band was used in all assays. Under these conditions, positive or negative modulation of DraG activity by the effector proteins GlnZ and AmtB could be determined. The relative upper and lower band intensities of each lane were determined by densitometry and quantitative analyses were performed with the IMAGEJ software [39]. For all conditions, the sum of the upper and lower bands was 100%.

The DraG activity in the presence of DraG only was calculated as follows:

$$\text{DraG only} = \frac{(\text{NCub} - \text{DraGub})}{\text{NCub}} \times 100$$

where NCub corresponds to the intensity of the Fe-protein upper band in the NC (absence of DraG), and DraGub corresponds to the intensity of the upper band in the presence of DraG.

The percentage of DraG activity was calculated as follows:

$$\% \text{DraG activity} = \left(\frac{\left(\frac{\text{NCub} - \text{Xub}}{\text{NCub}} \right) \times 100}{\text{DraG only}} \right) \times 100$$

where Xub corresponds to the intensity of the upper band in each condition evaluated, that is, presence or absence of GlnZ, AmtB, or GlnZΔ42-54. At least two independent experiments were performed for each condition. The data represent the mean ± SD.

To determine the effect of PII proteins on DraG activity, DraG concentration was kept constant in all reactions. GlnZ and AmtB concentrations are given relative to that of DraG. The molecular weights of the DraG and PII trimers were considered to be 32 and 36 kDa, respectively. AmtB was considered to be a trimer with a molecular weight of 134 kDa.

As the yield from the preparations of *A. brasilense* AmtB was not sufficient to achieve the concentrations needed in these reactions, we used AmtB from *E. coli*, which has 50% sequence identity with the *A. brasilense* homolog and is able to interact with *A. brasilense* GlnZ [18].

DraG activity was also determined indirectly by measuring the Fe-protein activity based on H_2 evolution under anaerobic conditions, as reported previously [16]. Firstly, *Azotobacter vinelandii* Fe-protein ADP-ribosylated *in vitro* or unmodified Fe-protein was incubated with DraG and then Fe-protein activity was determined by adding MoFe-protein. The ADP-ribosylated Fe-protein was produced by the incubation of purified Fe-protein (unmodified) with the *A. brasilense* DraT-GlnB complex. The reaction for 500 μL was carried out in buffer containing 50 mм MOPS pH 7.5, 5 mм ADP or ATP, 10 mм $MgCl_2$, 1 mм $MnCl_2$, 0.03% (w/v) Triton X-100 (TX), 150 μg of ADP-ribosylated or unmodified Fe-protein, 10 μg of His-tagged DraG, and different proportions of GlnZ and AmtB. *Azospirillum brasilense* AmtB was purified as previously described [19]. Nitrogenase activity buffer was kept as twice concentrated, containing 200 mм MOPS, 13.4 mм $MgCl_2$, 60 mм phosphocreatine, 10 mм ATP, 2.3 mg·mL^{-1} BSA, 0.4 mg·mL^{-1} creatine phosphokinase, and 24 mм dithionite. Immediately after incubation with DraG, 500 μL of this nitrogenase buffer was added to each vial, yielding 1-mL final reaction volume. To determine Fe-protein activity, MoFe-protein was added in a 1 : 1.4 molar ratio (MoFe : Fe-protein). The reaction mixtures were incubated for 20 min at 160 r.p.m. at 30 °C. H_2 evolution was measured by gas chromatography. For all reactions, DraG concentration was kept constant, while the GlnZ concentration varied up to 40-fold higher than that of DraG. AmtB was used in a slight molar excess, yielding a molar ratio of 1 : 40 : 1.2 DraG : GlnZ : AmtB, considering AmtB as trimer.

Intrinsic tryptophan fluorescence assay

Experiments were performed at 25 °C using a Cary Eclipse fluorescence spectrophotometer (Agilent, Santa Clara, CA, USA). All measurements were corrected for buffer contributions to the fluorescence. Purified proteins, at indicated concentrations in buffer (20 mм Tris pH 7.5, 50 mм NaCl, 0.03% (w/v) DDM, 5 mм ADP and 10 mм $MgCl_2$), were excited at 300 nm and emission was scanned from 310 to 400 nm. The experiments were repeated at least three times, and the most representative curve was fitted with the GRAPH PAD PRISM program (GraphPad, San Diego, CA, USA). For GlnZ titration with AmtB, the fluorescence of AmtB at 339.06 nm was recorded. Experimental data were fitted to the one-site specific binding model using the GRAPH PAD PRISM program to estimate the dissociation constant of the complex considering both AmtB and GlnZ as trimers.

Crystallization, data collection, structure determination, and refinement

The DraG-GlnZΔ42-54 complex was concentrated to 13 mg·mL^{-1} and was incubated with 5 mм ADP prior to crystallization. Crystallizations were performed by the vapor diffusion method using a Mosquito robot and commercially available screens. Hanging-drop setups containing 100 nL of protein and 100 nL of precipitant gave single well-diffracting crystals in several conditions. A merohedrally twinned crystal obtained with 35% (v/v) glycerol ethoxylate and 0.2 м lithium citrate in the well solution showed diffraction of highest quality and data to 1.55 Å resolution were collected in a nitrogen stream at beamline 14.1 at the BESSY II synchrotron in Berlin. Data processing and reduction were performed using XDS and programs from the CCP4 suite [40]. Several twin tests suggested twinning, with the twin operator k, h, -l, and an estimated twin fraction of 0.4. Phases were obtained by molecular replacement with the previously solved native DraG-GlnZ complex structure as model (PDB ID: 3O5T) using Molrep [41]. Intensity-based twin refinement in Refmac5 (5.8.0049) [42] was interspersed with rounds of manual model building in COOT [43]. Care was taken not to bias the refinement and twin-related reflections were kept in either the work or the test set. Phenix [44] was used to assign R_{free} in resolution shells. The R_{work} and R_{free} of the final model were 14.4% and 16.5%, respectively, and the twin fraction refined to 0.412. A summary of the data collection and refinement statistics can be found in Table 2. The model and structure factors have been deposited in the protein data band with PDB ID: 5OVO.

ITC measurements

All ITC experiments were performed on an iTC200 (GE Healthcare) at 25 °C in buffer I, which contained 50 mм Tris pH 7.5, 100 mм NaCl, 10 mм $MgCl_2$, 3 mм ADP, and 10% glycerol. ADP stock solution was freshly prepared and the pH was adjusted to 7.0. Purified GlnZ, GlnZΔ42-54, and DraG were dialyzed against buffer I. ADP-saturated DraG (30 μм) was titrated with 650 μм GlnZ and ADP-saturated DraG (90 μм) was titrated with 1050 μм of GlnZΔ42-54, considering all proteins as monomers, to allow the analysis using a one to one binding model. Data analysis was carried out using ORIGIN 7 (OriginLab, Northampton, MA, USA).

SPR measurements

A multiparametric SPR 220A instrument (BioNavis Instruments, Helsinki, Finland) was used to clean, immobilize, and detect variations in the refractive index at the interface of the sensor. Prior to protein immobilization, the sensor surface was cleaned with 2 м NaCl and 0.01 м NaOH solution. Covalent linkage of DraG to the carboxymethylated dextran matrix on the surface of the CMD 500 I, 3D sensor chip was achieved by amine coupling. Activation of the carboxyl groups on the matrix was performed by adding a mixture of succinimide (NHS) and carbodiimide (EDC) at

final concentrations of 0.05 and 0.2 M, respectively. DraG immobilization was achieved through injection of 0.1 mg·mL^{-1} DraG in 5 mM MES pH 5.0, during 7 min, followed by continuous flow of buffer I at 30 μL·min^{-1}. After the immobilization was achieved, a 1 M ethanolamine solution was injected to deactivate remaining active esters. Then, the sensor was washed with buffer I at 30 μL·min^{-1}. As NC for nonspecific interactions between the analyte and the sensor surface, diluted DraG buffer I was injected into the reference flow cell instead of DraG.

Measurements of interaction of GlnZ and GlnZΔ42-54 with DraG were carried out at room temperature using buffer I as the running buffer. GlnZ and GlnZΔ42-54 solutions from 0 to 200 μM were prepared by diluting the stock protein solutions at 650 and 1050 μM, respectively, in buffer I. After injection end point, both GlnZ and GlnZΔ42-54 dissociated rapidly from DraG. Regeneration solution (500 mM NaCl) was injected between samples. The affinity constants and binding kinetics were determined from the interaction measurements using SPR Navi™ Data Viewer and TraceDrawer for SPR Navi™ (BioNavis Ltd, Tampere, Finland).

RNA isolation and first-strand cDNA synthesis

Total RNA was extracted from *A. brasilense* strain FP2 grown under nitrogen-fixing conditions. TRI Reagent (Sigma) was used for RNA isolation and genomic DNA was removed with DNase I (Ambion, ThermoFisher Scientific, Waltham, MA, USA) before reverse transcription. The integrity and quality of the total RNA were confirmed by spectrophotometric analysis and agarose gel electrophoresis. cDNA was produced from 2 μg of DNase I-treated RNA using the high-capacity cDNA reverse transcription kit (Applied Biosystems, Foster City, CA, USA) according to the manufacturer's instruction, and the resulting cDNA was stored at −20 °C.

Quantification of mRNA levels by reverse transcription quantitative PCR

Reverse transcription qPCR was carried out using the SYBR Green PCR Master Mix and cDNA as template in a StepOne-Plus Real-Time PCR Detection System (both from Applied Biosystems), according to the manufacturer's instructions. Sets of specific primers were designed using the genome sequence of *A. brasilense* (sequences are in Table 1) and PRIMER EXPRESS software (ThermoFisher Scientific). A denaturing cycle was performed after each run to check for nonspecific amplification or contamination. RT-qPCR reactions using purified RNA without treatment with reverse transcriptase were used as control, and all samples were made in triplicate. Calibration curves for all primers were linear over four orders of magnitude (R^2 = 0.97–0.99), and efficiencies were 85% or higher. mRNA levels were normalized using *gyrA* 1, *glyA*, and

recA as reference [45] using GENORM 3.4 software [46]. Relative expression levels were estimated as described previously [47].

In vivo effects of GlnZΔ42-54

To assess the influence of GlnZ and GlnZΔ42-54, plasmids named pLAFRglnZ and pLAFRglnZΔT were constructed by subcloning *glnZ* and *glnZΔ42-54* genes from pET28a [16,33] into pLAFR3.18 as a *Xba*I-*Hind*III fragment. These plasmids were then transferred by conjugation to *A. brasilense* strains 7611 (*glnZ* mutant) and FAJ310 (*amtB* mutant). *Azospirillum brasilense* strains grown to saturation in NFbHP-lactate medium [48] supplemented with 20 mM NH$_4$Cl were used to inoculate 100 ml of NFbHP-lactate containing 5 mM sodium glutamate and 1% of LB medium in a 1 : 100 dilution in 250-mL flask, as described previously [49]. The cells were grown at 120 r.p.m. for ~ 24 h at 30 °C in a water bath incubator. Nitrogenase activity was determined in whole cells by the acetylene reduction assay. Ammonium shock was carried out by adding 200 μM NH$_4$Cl. At specific times of 1–20 min, samples were collected and transferred to SDS/PAGE sample buffer, as previously described [17], subjected to 12% low-cross-linking SDS/PAGE, followed by western blot using antibody against *A. brasilense* Fe-protein.

Acknowledgements

Author contributions

VRM, FOP, LCS, LFH, MH, SN, and EMS designed the research; VRM performed and analyzed the experiments shown in Figs 1–5, 9, and 10, provided technical assistance for experiments shown in Figs 6–8 and wrote the paper. CLBS performed and analyzed the experiments shown in Figs 6 and 7. GV provided technical assistance for the experiments shown in Figs 1 and 2. EN purified AmtB protein used in experiments shown in Fig. 2 and provided technical assistance for the experiment shown in Fig. 4. MASO performed and analyzed the experiment shown in Fig. 8. ECMG

provided technical assistance for the experiment shown in Fig. 8. FOP wrote the paper. DAM analyzed binding data. LCS analyzed the experiment shown in Fig. 5. MH analyzed the experiments shown in Figs 6 and 7. SN analyzed the experiments shown in Figs 2 and 3. EMS analyzed the experiments shown in Figs 1–5, 9, and 10. LCS, LFH, SN and EMS contributed to the writing of the paper.

References

1 Dixon R & Kahn D (2004) Genetic regulation of biological nitrogen fixation. *Nat Rev Microbiol* **2**, 621–631.

2 Seefeldt LC, Hoffman BM & Dean DR (2009) Mechanism of Mo-dependent nitrogenase. *Annu Rev Biochem* **78**, 701–722.

3 Huergo LF, Pedrosa FO, Muller-Santos M, Chubatsu LS, Monteiro RA, Merrick M & Souza EM (2012) PII signal transduction proteins: pivotal players in post-translational control of nitrogenase activity. *Microbiology* **158**, 176–190.

4 Nordlund S & Högbom M (2013) ADP-ribosylation, a mechanism regulating nitrogenase activity. *FEBS J* **280**, 3484–3490.

5 Moure VR, Costa FF, Cruz LM, Pedrosa FO, Souza EM, Li X-D, Winkler F & Huergo LF (2015) Regulation of nitrogenase by reversible mono-ADP-ribosylation. *Curr Top Microbiol Immunol* **384**, 89–106.

6 Huergo LF, Chandra G & Merrick M (2013) PII signal transduction proteins: nitrogen regulation and beyond. *FEMS Microbiol Rev* **37**, 251–283.

7 Jiang P & Ninfa AJ (2009) Sensation and signaling of α-ketoglutarate and adenylylate energy charge by the *Escherichia coli* PII signal transduction protein require cooperation of the three ligand-binding sites within the PII trimer. *Biochemistry (Mosc.)* **48**, 11522–11531.

8 Truan D, Bjelić S, Li X-D & Winkler FK (2014) Structure and thermodynamics of effector molecule binding to the nitrogen signal transduction PII protein GlnZ from *Azospirillum brasilense*. *J Mol Biol* **426**, 2783–2799.

9 Truan D, Huergo LF, Chubatsu LS, Merrick M, Li XD & Winkler FK (2010) A new PII protein structure identifies the 2-oxoglutarate binding site. *J Mol Biol* **400**, 531–539.

10 Maier S, Schleberger P, Lü W, Wacker T, Pflüger T, Litz C & Andrade SLA (2011) Mechanism of disruption of the Amt-GlnK complex by PII-mediated sensing of 2-oxoglutarate. *PLoS ONE* **6**, e26327.

11 Fokina O, Chellamuthu V-R, Forchhammer K & Zeth K (2010) Mechanism of 2-oxoglutarate signaling by the *Synechococcus elongatus* PII signal transduction protein. *Proc Natl Acad Sci* **107**, 19760–19765.

12 Huergo LF, Chubatsu LS, Souza EM, Pedrosa FO, Steffens MBR & Merrick M (2006) Interactions between PII proteins and the nitrogenase regulatory enzymes DraT and DraG in *Azospirillum brasilense*. *FEBS Lett* **580**, 5232–5236.

13 Huergo LF, Merrick M, Pedrosa FO, Chubatsu LS, Araujo LM & Souza EM (2007) Ternary complex formation between AmtB, GlnZ and the nitrogenase regulatory enzyme DraG reveals a novel facet of nitrogen regulation in bacteria. *Mol Microbiol* **66**, 1523–1535.

14 Huergo LF, Merrick M, Monteiro RA, Chubatsu LS, Steffens MBR, Pedrosa FO & Souza EM (2009) *In vitro* interactions between the PII proteins and the nitrogenase regulatory enzymes dinitrogenase reductase ADP-ribosyltransferase (DraT) and dinitrogenase reductase-activating glycohydrolase (DraG) in *Azospirillum brasilense*. *J Biol Chem* **284**, 6674–6682.

15 Gerhardt ECM, Araujo LM, Ribeiro RR, Chubatsu LS, Scarduelli M, Rodrigues TE, Monteiro RA, Pedrosa FO, Souza EM & Huergo LF (2012) Influence of the ADP/ATP ratio, 2-oxoglutarate and divalent ions on *Azospirillum brasilense* PII protein signalling. *Microbiology* **158**, 1656–1663.

16 Moure VR, Danyal K, Yang Z-Y, Wendroth S, Müller-Santos M, Pedrosa FO, Scarduelli M, Gerhardt ECM, Huergo LF, Souza EM *et al.* (2013) The nitrogenase regulatory enzyme dinitrogenase reductase ADP-ribosyltransferase (DraT) is activated by direct interaction with the signal transduction protein GlnB. *J Bacteriol* **195**, 279–286.

17 Huergo LF, Souza EM, Araujo MS, Pedrosa FO, Chubatsu LS, Steffens MBR & Merrick M (2006) ADP-ribosylation of dinitrogenase reductase in *Azospirillum brasilense* is regulated by AmtB-dependent membrane sequestration of DraG. *Mol Microbiol* **59**, 326–337.

18 Rajendran C, Gerhardt ECM, Bjelic S, Gasperina A, Scarduelli M, Pedrosa FO, Chubatsu LS, Merrick M, Souza EM, Winkler FK *et al.* (2011) Crystal structure of the GlnZ-DraG complex reveals a different form of PII-target interaction. *Proc Natl Acad Sci* **108**, 18972–18976.

19 Rodrigues TE, Souza VEP, Monteiro RA, Gerhardt ECM, Araújo LM, Chubatsu LS, Souza EM, Pedrosa FO & Huergo LF (2011) *In vitro* interaction between the ammonium transport protein AmtB and partially uridylylated forms of the P(II) protein GlnZ. *Biochim Biophys Acta* **1814**, 1203–1209.

20 Li X-D, Winkler FK & Huergo LF (2015) How does the DraG–PII complex regulate nitrogenase activity in *Azospirillum brasilense*? In Biological Nitrogen Fixation (de Bruijn FJ, ed), pp. 139–146. John Wiley & Sons, Inc, Hoboken, NY.

21 Conroy MJ, Durand A, Lupo D, Li X-D, Bullough PA, Winkler FK & Merrick M (2007) The crystal

structure of the *Escherichia coli* AmtB-GlnK complex reveals how GlnK regulates the ammonia channel. *Proc Natl Acad Sci USA* **104**, 1213–1218.

22 Li X-D, Huergo LF, Gasperina A, Pedrosa FO, Merrick M & Winkler FK (2009) Crystal structure of dinitrogenase reductase-activating glycohydrolase (DRAG) reveals conservation in the ADP-ribosylhydrolase fold and specific features in the ADP-ribose-binding Pocket. *J Mol Biol* **390**, 737–746.

23 Berthold CL, Wang H, Nordlund S & Högbom M (2009) Mechanism of ADP-ribosylation removal revealed by the structure and ligand complexes of the dimanganese mono-ADP-ribosylhydrolase DraG. *Proc Natl Acad Sci* **106**, 14247–14252.

24 Ahmed MH, Spyrakis F, Cozzini P, Tripathi PK, Mozzarelli A, Scarsdale JN, Safo MA & Kellogg GE (2011) Bound water at protein-protein interfaces: partners, roles and hydrophobic bubbles as a conserved motif. *PLoS ONE* **6**, e24712.

25 Dunitz JD (1994) The entropic cost of bound water in crystals and biomolecules. *Science* **264**, 670.

26 Hota PK & Buck M (2009) Thermodynamic characterization of two homologous protein complexes: associations of the semaphorin receptor plexin-B1 RhoGTPase binding domain with Rnd1 and active Rac1. *Protein Sci* **18**, 1060–1071.

27 Klassen G, De Souza EM, Yates MG, Rigo LU, Inaba J & de Oliveira Pedrosa F (2001) Control of nitrogenase reactivation by the GlnZ protein in *Azospirillum brasilense*. *J Bacteriol* **183**, 6710.

28 Yakunin AF & Hallenbeck PC (2002) AmtB is necessary for NH4+-induced nitrogenase switch-off and ADP-ribosylation in *Rhodobacter capsulatus*. *J Bacteriol* **184**, 4081–4088.

29 Martin DE & Reinhold-Hurek B (2002) Distinct roles of P(II)-like signal transmitter proteins and amtB in regulation of nif gene expression, nitrogenase activity, and posttranslational modification of NifH in *Azoarcus* sp. strain BH72. *J Bacteriol* **184**, 2251–2259.

30 Zhang Y, Pohlmann EL, Ludden PW & Roberts GP (2001) Functional characterization of three GlnB homologs in the photosynthetic bacterium *Rhodospirillum rubrum*: roles in sensing ammonium and energy status. *J Bacteriol* **183**, 6159–6168.

31 Huergo LF, Souza EM, Steffens MBR, Yates MG, Pedrosa FO & Chubatsu LS (2005) Effects of over-expression of the regulatory enzymes DraT and DraG on the ammonium-dependent post-translational regulation of nitrogenase reductase in *Azospirillum brasilense*. *Arch Microbiol* **183**, 209–217.

32 Selao TT, Nordlund S & Norén A (2008) Comparative proteomic studies in *Rhodospirillum rubrum* grown under different nitrogen conditions. *J Proteome Res* **7**, 3267–3275.

33 Moure VR, Razzera G, Araújo LM, Oliveira MAS, Gerhardt ECM, Müller-Santos M, Almeida F, Pedrosa FO, Valente AP, Souza EM *et al.* (2012) Heat stability of proteobacterial PII protein facilitate purification using a single chromatography step. *Protein Expr Purif* **81**, 83–88.

34 Daley DO, Rapp M, Granseth E, Melén K, Drew D & von Heijne G (2005) Global topology analysis of the *Escherichia coli* inner membrane proteome. *Science* **308**, 1321–1323.

35 Drew D, Lerch M, Kunji E, Slotboom D-J & de Gier J-W (2006) Optimization of membrane protein overexpression and purification using GFP fusions. *Nat Methods* **3**, 303–313.

36 Lee C, Kang HJ, Hjelm A, Qureshi AA, Nji E, Choudhury H, Beis K, de Gier J-W & Drew D (2014) MemStar: a one-shot *Escherichia coli*-based approach for high-level bacterial membrane protein production. *FEBS Lett* **588**, 3761–3769.

37 Lucast LJ, Batey RT & Doudna JA (2001) Large-scale purification of a stable form of recombinant *tobacco etch virus* protease. *Biotechniques* **30**, 544–546, 548, 550 passim.

38 Kanemoto RH & Ludden PW (1984) Effect of ammonia, darkness, and phenazine methosulfate on whole-cell nitrogenase activity and Fe protein modification in *Rhodospirillum Rubrum*. *J Bacteriol* **158**, 713–720.

39 Schneider CA, Rasband WS & Eliceiri KW (2012) NIH Image to ImageJ: 25 years of image analysis. *Nat methods* **9**, 671–675.

40 Collaborative Computational Project, Number 4 (1994) The CCP4 suite: programs for protein crystallography. *Acta Crystallogr D Biol Crystallogr* **50**, 760–763.

41 Vagin A & Teplyakov A (1997) MOLREP: an automated program for molecular replacement. *J Appl Crystallogr* **30**, 1022–1025.

42 Murshudov GN, Vagin AA & Dodson EJ (1997) Refinement of macromolecular structures by the maximum-likelihood method. *Acta Crystallogr D Biol Crystallogr* **53**, 240–255.

43 Emsley P & Cowtan K (2004) Coot: model-building tools for molecular graphics. *Acta Crystallogr D Biol Crystallogr* **60**, 2126–2132.

44 Adams PD, Grosse-Kunstleve RW, Hung LW, Ioerger TR, McCoy AJ, Moriarty NW, Read RJ, Sacchettini JC, Sauter NK & Terwilliger TC (2002) PHENIX: building new software for automated crystallographic structure determination. *Acta Crystallogr D Biol Crystallogr* **58**, 1948–1954.

45 McMillan M & Pereg L (2014) Evaluation of reference genes for gene expression analysis using quantitative RT-PCR in *Azospirillum brasilense*. *PLoS ONE* **9**, e98162.

46 Vandesompele J, De Preter K, Pattyn F, Poppe B, Van Roy N, De Paepe A & Speleman F (2002) Accurate normalization of real-time quantitative RT-PCR data by geometric averaging of multiple internal control genes. *Genome Biol* **3**, 1–12.

47 Pfaffl MW (2001) A new mathematical model for relative quantification in real-time RT–PCR. *Nucleic Acids Res* **29**, e45.

48 Machado HB, Funayama S, Rigo LU & Pedrosa FO (1991) Excretion of ammonium by *Azospirillum brasilense* mutants resistant to ethylenediamine. *Can J Microbiol* **37**, 549–553.

49 Santos KFDN, Moure VR, Hauer V, Santos ARS, Donatti L, Galvão CW, Pedrosa FO, Souza EM, Wassem R & Steffens MBR (2016) Wheat colonization by an A*zospirillum brasilense* ammonium-excreting strain reveals upregulation of nitrogenase and superior plant growth promotion. *Plant Soil*, **415**, 245–255.

50 Camilios-Neto D, Bonato P, Wassem R, Tadra-Sfeir MZ, Brusamarello-Santos LC, Valdameri G, Donatti L, Faoro H, Weiss VA, Chubatsu LS *et al.* (2014) Dual RNA-seq transcriptional analysis of wheat roots colonized by *Azospirillum brasilense* reveals up-regulation of nutrient acquisition and cell cycle genes. *BMC Genom* **15**, 378.